Journal of Molecular Structure 1086 (2015) 153–160

Contents lists available at ScienceDirect

Journal of Molecular Structure

journal homepage: www.elsevier.com/locate/molstruc

Synthesis, spectral, X-ray single structure, DFT calculations and antimicrobial activities of [$Co^{(II)}X_2$ (dmphen)] (X = Br and SCN^-)

Mousa Al-Noaimi [a,*], Firas F. Awwadi [b], Salim F. Haddad [b], Wamidh H. Talib [c], Shehdeh Jodeh [d], Smaail Radi [e], Taibi Ben Hadda [e], Muneer Abdoh [f], S. Naveen [g], N.K. Lokanath [h], Ismail Warad [d,*]

[a] Department of Chemistry, Hashemite University, Zarqa 13115, Jordan
[b] Chemistry Department, Faculty of Science, The University of Jordan, Amman 11942, Jordan
[c] Department of Clinical Pharmacy and Therapeutics, Applied Science University, Amman 11931, Jordan
[d] Department of Chemistry, Science College, An-Najah National University, P.O. Box 7, Nablus, State of Palestine
[e] Lab of Chemical Material, FSO, University Mohammed Premier, Oujda 60000, Morocco
[f] Department of Physics, Science College, An-Najah National University, P.O. Box 7, Nablus, State of Palestine
[g] Institution of Excellence, Vijnana Bhavana, University of Mysore, Manasagangotri, Mysore 570 006, India
[h] Department of Studies in Physics, University of Mysore, Manasagangotri, Mysore 570 006, India

HIGHLIGHTS

- Two cobalt(II) complexes of type [$Co(X)_2$(dmphen)] (X = Br, NCS) were synthesized.
- Antimicrobial properties of these complexes were assessed.
- X-ray crystal structures for the two complexes were described.
- The absorption spectrum of these complexes in acetone was modeled (TD-DFT).

GRAPHICAL ABSTRACT

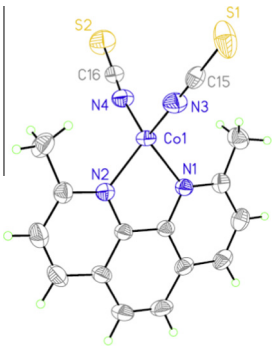

ARTICLE INFO

Article history:
Received 27 August 2014
Received in revised form 21 December 2014
Accepted 22 December 2014
Available online 16 January 2015

Keywords:
Co(II) complex
Single crystal structure
2,9-Dimethyl-1,10-phenanthroline
DFT calculations

ABSTRACT

Two tetrahedral mononuclear complexes with a general formula [CoX_2(dmphen)](**1–2**) (where dmphen is 2,9-dimethyl-1,10-phenanthroline and **1** (X = Br), **2** (X = NCS)) have been synthesized. These complexes are characterized by elemental analysis, IR, UV–visible, TG/DTA and by X-ray diffraction. The calculated electrostatic potential surface of 2 has shown that the electrostatic potential values around sulfur atom is anistropically distributed; the potential values along C–S bond is less negative than the corresponding values in the π-region of S atom. This agrees with the observed geometrical arrangement of C–H···S–C hydrogen bonding interactions, the avg. of H···S–C angle is 81°. Antimicrobial properties of cobalt(II) complexes was also assessed. Cobalt complexes exhibited significant antibacterial activity against different gram negative and positive human pathogens. The absorption spectrum of these complexes in acetone was modeled by time-dependent density functional theory (TD-DFT).

© 2014 Elsevier B.V. All rights reserved.

Introduction

1,l0-Phenanthroline and their derivatives are good π-acceptor ligands and can form stable complexes with a wide variety of metal

* Corresponding authors. Tel.: +962 (5) 3903333; fax: +962 (5) 3826613.
E-mail addresses: manoaimi@hu.edu.jo (M. Al-Noaimi), warad@najah.edu (I. Warad).

http://dx.doi.org/10.1016/j.molstruc.2014.12.071
0022-2860/© 2014 Elsevier B.V. All rights reserved.

ions. The resulting complexes are high stabile due to the $d\pi \rightarrow p\pi$ back donation [1–3]. These complexes have been studied due to their potential applications as anticancer and antimicrobial agents, DNA foot printing agents and their ability to probe the structure of DNA [4–6]. Also, these complexes have potential to bind and cleave the DNA via a multitude of interactions [7–9].

The construction of coordination compounds of cobalt(II) is the center of attraction due to interesting structural and physicochemical properties [10–12]. Utsuno and coworkers have studied the structures of a series of $[Co(phen)_2X_2]^{n+}$ (X = CN^-, NO–; Br–, SCN^-) complexes, by ^{13}C NMR spectra [13]. The crystal structures of some cobalt complexes with phen containing other ligands have been studied, such as $[Co(phen)_2(CO_3))]Br{\cdot}4H_2O$ [14].

Recently, we have reported the syntheses, structural characterizations and molecular properties of several mononuclear [15] and dinuclear [16] complexes using 2,9-dimethyl-1,10-phenanthrolines as bidentate ligands. We also reported that complexes of general formula $[MX_2(dmphen)]$ found to be very suitable precursors to prepare regular spherical nanoparticles metal oxide through low temperature thermal decomposition [17]. Herein, we report synthesis and characterization of two cobalt(II) complexes. The reactions were monitored by IR and UV–vis. Complexes **'1** and **2'** have been structurally characterized by X-ray crystallography. The thermal activity of complexes **'1** and **2'** was evaluated by TG/DTA. The antimicrobial properties of these complexes (**1–2**) were also assessed with two gram negative and two gram positive bacterium. The calculated electrostatic potential was used to rationalize the self-assembly of the two complexes. The absorption spectrum of **1** in acetone was modeled by time-dependent density functional theory (TD-DFT).

Experimental

Material and instrumentation

2,9-Dimethyl-1,10-phenanthroline ligand, $CoBr_2{\cdot}6H_2O$ and $Co(NCS)_2$ were purchased from across. Elemental analyses were carried out on an Elementar Vario EL analyzer. And the IR spectra for the complexes were recorded using Perkin Elmer Spectrum 1000 FT-IR Spectrometer. UV–visible spectra were measured using TU-1901 double-beam UV–visible spectrophotometer in acetone as solvent.

General procedure for complex $[CoX_2(dmphen)]$ (1–2)

A mixture of CoX_2 salt (2 mmol) in distilled ethanol (15 mL) and free ligand (2.1 mmol) in ethanol (10 mL) was stirred for around 0.5 h at room temperature until the precipitation appeared. The solid was filtered, washed with ethanol and dried. Suitable crystals for X-ray diffraction analysis were grown by slow evaporation of a solution of the complex in mixture of (1:1) ethanol:CH_2Cl_2 solvent after two days.

*$[CoX_2(dmphen)]$ (**1**)*

Yield: 0.77 g (90%). Anal. Calc. for $C_{14}H_{12}Br_2CoN_2$: C, 39.38; H, 2.83; N, 6.56. Found. C, 39.30; H, 2.81; N, 6.49. UV–vis (nm) bands in dichloromethane: 645, 617, 555, 357, 280 and 240.

*$[Co(NCS)_2(dmphen)]$ (**2**)*

Yield: 0.67 g (88%). Anal. Calc. for $C_{16}H_{12}CoN_4S_2$: C, 50.13; H, 3.16; N, 14.61; S, 16.73 Found. C, 50.02; H, 3.10; N, 14.53; S, 16.56. UV–vis (nm) bands in dichloromethane: 666, 635, 570, 242, and 282.

Crystallography

A suitable single crystal from complexes **'1** and **2'** was chosen for an X-ray diffraction measurement. For complex **1**, X-ray intensity data were collected at 296 K on a Bruker CCD diffractometer equipped with Cu Kα radiation (l = 1.54178 Å). Data reduction of all the collected reflections and absorption correction were carried out using the APEX 2 [18] package. For complex **2** The diffraction data sets were collected at room temperature employing enhanced Mo radiation, k = 0.71073 Å, using Xcalibur/Oxford Diffractometer equipped with Eos CCD detector. CrysAlisPro software was used for data collection, absorption correction and data reduction to give *hkl* files [19]. The structures were solved using SHELXTL program package [20]. All nonhydrogen atoms were refined anisotropically. Hydrogen atoms were placed in calculated positions and refined using a riding model. Details of data collection and refinement are given in Table 1.

Antibacterial assay

The antibacterial activity of the investigated complexes **'1** and **2'** was tested against the following human pathogens: *Escherichia coli* (ATCC 25922), *Staphylococcus aureus* (ATCC 25213), *Pseudomonas aeruginosa* (ATCC 27853), and *Bacillus subtilis* (ATCC 6633) using disk diffusion method [21,22]. Bacterial strains were cultured overnight in Muller Hinton broth (Oxoid, UK) and the turbidity was adjusted to a concentration equal to 0.5 McFarland standards. One hundred microliter of the bacterial suspension was used to inoculate Muller Hinton agar plates. Stock compounds were initially dissolved in DMSO and diluted using Muller Hinton broth so that the final concentration of DMSO in filter disks is less that 1%. Sterilized filter disks (6 mm) were impregnated with 25 μl of 1 mg/ml of the complex and placed onto cultured plates followed by incubation at 37 °C for 24 h then inhibition zones were measured in millimeters. Filters containing 1 mg/ml tetracycline were used as a positive control and filters with 1% DMSO were used as a negative control. All tests were performed in triplicates.

Theoretical calculations

Full geometry optimization of **'1** and **2'** were carried out using density functional theory (DFT) at the B3LYP level [23]. All calculations were carried out using the GAUSSIAN 09 program package with the aid of the GaussView visualization program [24]. For C, H and N the cc-pvdz basis set were assigned, while for Cu, the LanL2DZ basis set with effective core potential were employed [25]. Vertical electronic excitations based on B3LYP optimized geometries were computed using the time-dependent density functional theory (TD-DFT) formalism in acetone using polarizable continuum model (PCM) [26–29]. Gauss Sum was used to calculate the fractional contributions of various groups to each molecular orbital [30].

Results and discussions

*Synthesis of the desired complexes **'1** and **2'***

The mononuclear complexes (**1–2**) were isolated in an excellent yield without side products by stirring equivalent amounts of dmphen with $CoBr_2{\cdot}6H_2O$ or $Co(NCS)_2$ in ethanol (Scheme 1). The reactions were monitored by IR and UV–visible spectroscopy and the structure of complexes **'1** and **2'** were confirmed by X-ray diffraction.

IR spectra of complexes **'1** and **2'** (Fig. 1) showed four main sets of characteristic absorption bands in the range 2965 and

Table 1
Crystal data and structure refinement for complexes '**1** and **2**'.

	Complex **1**	Complex **2**
Empirical formula	$C_{14}H_{12}Br_2CoN_2$	$C_{16}H_{12}CoN_4S_2$
Formula weight	427.01	383.35
Temperature	293(2) K	296(2) K
Wavelength	0.71073 Å	1.54178 Å
Crystal system	Monoclinic	Monoclinic
Space group	$P2_1/c$	$P2_1/n$
Unit cell dimensions	a = 9.4204(7) Å	a = 8.5103(4) Å
	b = 18.3537(11) Å	b = 13.7676(7) Å
	c = 9.3743(10) Å	c = 14.5716(7) Å
Volume	1493.7(2) Å^3	1704.87(14) Å^3
Z	4	4
Density (calculated)	1.899 mg/m^3	1.494 mg/m^3
Absorption coefficient	6.485 mm^{-1}	10.201 mm^{-1}
F(000)	828	780
Theta range for data collection	3.23–26.30°	4.42–64.70°
Index ranges	$-11 <= h <= 7$, $-22 <= k <= 20$, $-10 <= l <= 10$	$-5 <= h <= 9$, $-15 <= k <= 15$, $-16 <= l <= 16$
Reflections collected	4025	19,054
Independent reflections	2411 [R(int) = 0.0414]	2802 [R(int) = 0.0498]
Data/restraints/parameters	2411/0/174	2802/0/210
Goodness-of-fit on F^2	1.004	1.057
Final R indices [I > 2sigma(I)]	[a]R_1 = 0.0528, [b]wR_2 = 0.1158	[a]R_1 = 0.0422, [b]wR_2 = 0.1152
R indices (all data)	[a]R_1 = 0.0780, [b]wR_2 = 0.1305	[a]R_1 = 0.0457, [b]wR_2 = 0.1182
Largest diff. peak and hole	0.595 and −0.562 e Å^{-3}	0.311 and −0.508 e Å^{-3}

[a] $R_1 = \Sigma||F_o| - |F_c||/\Sigma|F_o|$.
[b] $wR_2 = \left\{\Sigma\left[w\left(F_o^2 - F_c^2\right)^2\right]\Big/\Sigma\left[w\left(F_o^2\right)^2\right]\right\}^{1/2}$.

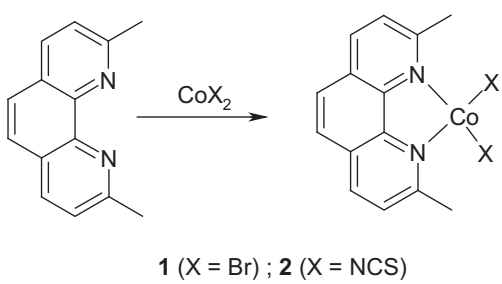

Scheme 1. Synthesis of the Co-complexes.

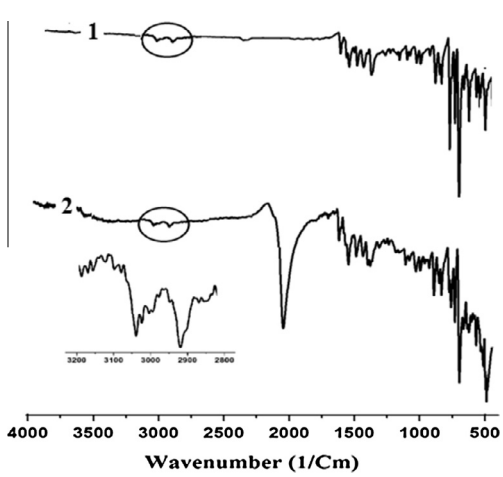

Fig. 1. IR-KBr disk spectra of the desired complexes '**1** and **2**'.

2850 cm^{-1} which can be assigned to H–Ph and H–CH_3 stretching vibrations, respectively. The C–H stretching vibrations of the aromatic ring appear at 3070 and 3020 cm^{-1} for complex **1**. The bands in the range 1673–1413 cm^{-1} are characteristics for the skeletal vibrations of the aromatic rings. The bands in the 1000–1372 cm^{-1} region can be assigned to the C–H in-plane bending bands. The absorption at 727 and 726 cm^{-1} corresponds to the out-of-plane bending vibrations of aromatic rings. The appearance of SCN stretching vibration at 2200 cm^{-1} is a characteristic for the synthesis of complex **2**.

*Thermal decomposition analysis of complexes **1***

The thermal properties TG/DTA of the complex **1** was investigated under an open atmosphere in the range of 0–800 °C and heating rate of 10 °C/min. Fig. 2 shows that there are no uncoordinated or coordinated water molecules upon heating complex **1** within the range 0–150 °C. Decomposition study of complex **1** showed no intermediate decomposition steps of the coordinated bromides and dmphen ligands, both ligands de-structured away from the complex with one broad step decomposition in 260–480 °C with weight loss ~78% and an exothermic DTA signal at ~380 °C.

X-ray single crystal of CoX_2(dmphen) complexes

The selected bond lengths and bond angles for complexes **1** (Fig. 3) and **2** (Fig. 4) are given in Table 2. Complex **1** has a discrete mononuclear structure. As depicted in Fig. 3, the cobalt atom is coordinated by dmphen ligand and two bromide ions. The cobalt

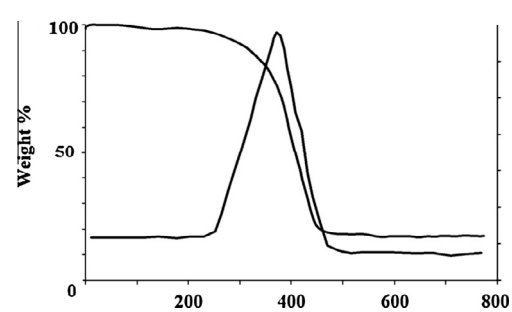

Fig. 2. TG/DTA thermal curves of the desired complexes **1**.

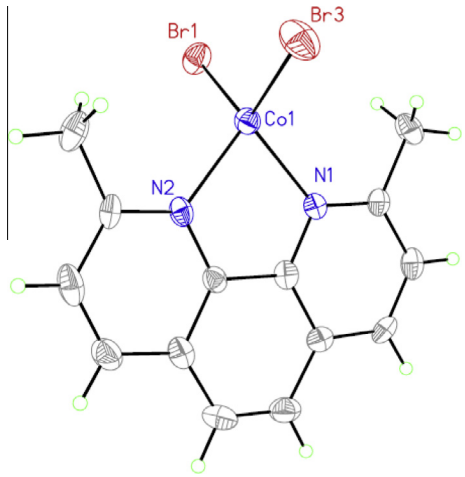

Fig. 3. Molecular structure complex **1**. Thermal ellipsoids are drawn at the 50% probability level [20].

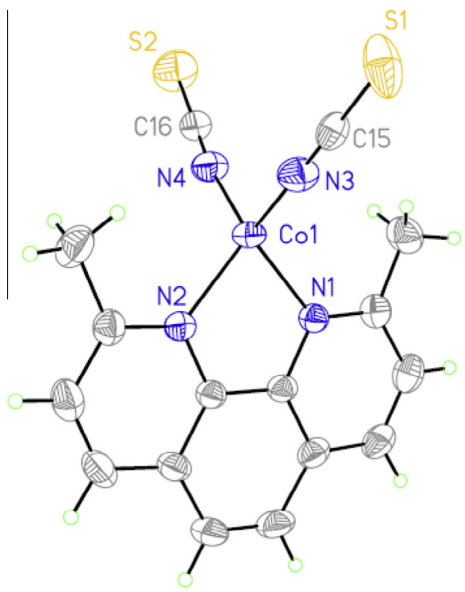

Fig. 4. Molecular structure of complex **2**. Thermal ellipsoids are drawn at the 50% probability level [20].

atom is four-coordinated by two pyridyl N atoms (N(1) and N(2) atoms) and two bromide atom (Br(1) and Br(3)) in a distorted tetraheral geometry with Co–N bond lengths falling in the 2.044(6) Å and 2.048(4) Å for Co1–N1 and Co1–N2, Co–Br bond lengths of 2.3665(11) and 2.3350(0) Å, and N/Br–Co–N/Br bond angles varying from 81.9(2)° to 115.98(5)° (Table 2). A solvate structure of **1** is reported in the literature [31]. The lattice includes water and a methanol molecule, the average Co–Br distance in **1** is less than the corresponding solvate; Co–Br average distance is 2.397 Å in the solvate, whereas it is 2.351 Å in **1**. Moreover, the Br–Co–Br angle in **1** is less than the corresponding distance in the solvate; these angles are 115.98° and 118.28° for **1** and the solvate. These differences can be rationalized using the fact that the Br ligand is involved in Br···H–O strong hydrogen interactions in the solvate, whereas this strong interaction is absent in **1**. It has been shown that intermolecular forces affect the molecular structure [32].

Complex **2** has a similar structure to that of complex **1**. As depicted in Fig. 4. The Co(II) atom is four-coordinated in a distorted tetrahedral configuration by two N atoms from one dmphen ligand and two thiocyanate ions. The Co–N of bond lengths of dmphen are 2.019(2) Å and 2.025(2) Å for Co1–N1 and Co1–N2 (Table 2 and Fig. 4) which are close to those in complex **1** (*vide supra*), whereas the corresponding Co–N bond distances of isothiocynate ligand are shorter by 0.1 Å (Table 2), this reflects the coordinating strength of this ligand.

The structure of the complexes **'1** and **2'** are optimized in gas phase and in acetone at B3LYP level using cc-pvdz basis sets on all atoms except Co and Br, LANL2DZ has been assigned to Co and Br atoms. Selected optimized distances and angles are listed in Table 2. The optimized distances are in good a agreement with the corresponding experimental values (the difference is less than 0.1 Å) except for the Co–Br distances in acetone (Table 2). These differences may be due to that the intermolecular forces in solid state have effects on the molecular structure [31,32]. Also, theoretical calculations are more accurate in prediction structural parameters when light atoms are involved in the bonds, the Co–N bond distances are in better agreement with the experimental ones than Co–Br distances.

The supramolecular structure of both complexes is developed mainly based on the C–H···A (A = proton acceptor) non-classical hydrogen bonding interactions and π–π interactions. Proton acceptors include bromide ligand in **1** or S atom in **2** (Fig. 5). Data summarizing these interactions are listed in Tables 3 and 4. In **2**, it is noteworthy that H···S–C is less than 90° in the two observed hydrogen bonding interactions. Olex2 program [33] was used to analyze π–π interactions. The interaction parameters are

Table 2
Selected bond lengths and angles for the complexes **'1** and **2'**.

Complex **1** Bond distances (Å)				Complex **2** Bond distances (Å)			
Bond	Experimental	Optimized (gas)	Optimized (acetone)	Bond	Experimental	Optimized (gas)	Optimized (acetone)
Br(1)–Co	2.3665(11)	2.43848	2.5154	Co(1)–N(3)	1.917(3)	1.91208	1.912
Co–N(1)	2.044(6)	2.10190	2.1031	Co(1)–N(1)	1.925(3)	1.91207	1.912
Co–N(2)	2.048(4)	2.10186	2.10641	Co(1)–N(4)	2.019(2)	2.11291	2.113
Co–Br(3)	2.3350(10)	2.43839	2.5102	Co(1)–N(2)	2.025(2)	2.11291	2.113
Bond angles (°)				Bond angles (°)			
Angle	Experimental	Optimized (gas)	Optimized (acetone)	Angle	Experimental	Optimized (gas)	Optimized (acetone)
N(1)–Co–N(2)	81.90(2)	80.91969	81.65	N(3)–Co(1)–N(1)	109.82(12)	125.25519	125.24
N(1)–Co–Br(3)	114.51(13)	111.42427	114.68	N(3)–Co(1)–N(4)	113.96(10)	110.75922	110.74
N(2)–Co–Br(3)	112.22(13)	111.33880	115.33	N(1)–Co(1)–N(4)	115.30(10)	110.39968	110.75
N(1)–Co–Br(1)	113.08(12)	111.39885	113.41	N(3)–Co(1)–N(2)	117.55(10)	110.40290	110.74
N(2)–Co–Br(1)	114.56(15)	111.39885	115.33	N(1)–Co(1)–N(2)	115.21(11)	110.76180	110.75
Br(3)–Co–Br(1)	115.98(5)	122.73550	114.27	N(4)–Co(1)–N(2)	82.94(9)	80.26255	80.27

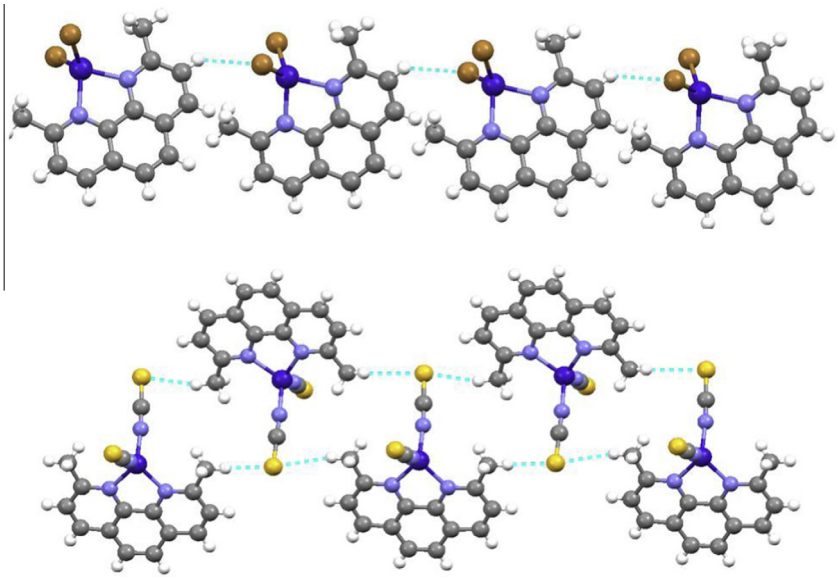

Fig. 5. Hydrogen bond interaction in **1** (above) and **2** (below).

Table 3
Hydrogen bond distances (Å) and angles (°).

Compound	C···A[a]	H···A	C–H···A	H···A–B[b]
1	3.728	2.969	139.64	140.61
2	3.723	2.820	157.10	76.14
2	3.637	2.915	132.2	85.83

[a] A = proton acceptor, bromide ligand in 1 and sulfur atom of SCN^- in 3.
[b] B = Co in 1 and C in 3.

Table 4
π–π interactions distance (Å).

Compound	Angle	Centroid–centroid distance	Shift distance
1	0	3.586	1.333
1	1.540	3.637	1.462
2	0	3.711	1.092
2	1.071	3.807	1.382

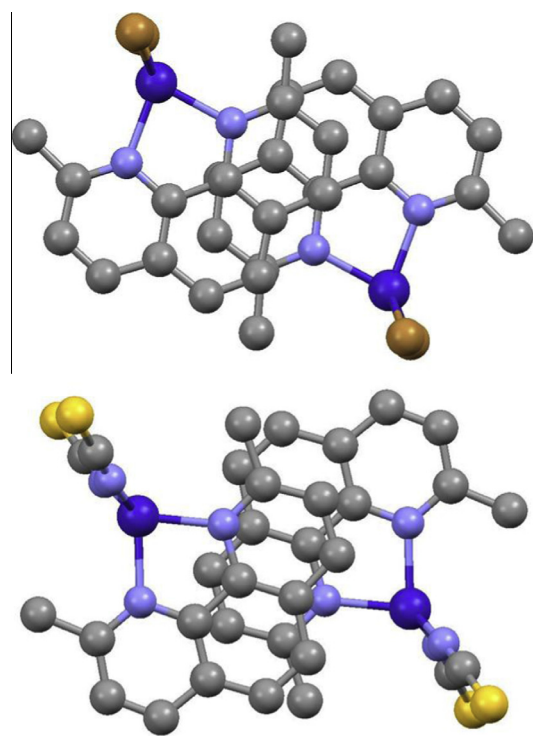

Fig. 6. Illustration of π–π interaction in **1** (above) and **2** (below).

summarized in Table 4. In both structures, the aromatic system is involved in π–π interactions (Fig. 6); one pyridyl ring is overlapped with phenyl and pyridyl rings from another symmetry related aromatic system. The centroid–centroid distances and shift distances (Table 4 and Fig. 6) indicate that the role π–π interactions in self-assembly of **1** (Fig. 6, above) is more significant than in **2** (Fig. 6, below). C–H···Br hydrogen bonding interactions connects the molecular units to form chain structures extend parallel to [701] crystallographic directions (Fig. 5, above). Whereas, C–H···S hydrogen bonding interactions links the molecular units of 3 to form chain structures run in *b* direction (Fig. 5, below). Subsequently, the chains of both compounds stack via π–π interactions and other weaker interactions to from the three-dimensional structure.

The supramolecular structure is rationalized using molecular electrostatic potential. The electrostatic potential surface for **'1** and **2'** was calculated at B3LYP level with cc-pvdz basis set on C, H, N and S, and LANL2DZ on Br and Co (Fig. 7) using G09 program package [29]. The coordinates of both molecules were extracted from the experimental structure. As expected, in **1**, the most negative electrostatic potential values are around the bromide ligand and most positive values are around the hydrogen atoms, this rationalizes the formation (Fig. 7(right)) of the C–H···Br hydrogen bonding interactions. Similarly, the most positive electrostatic potential values are around H atoms in 2. While electrostatic potential around S atom is negative, interestingly, the electrostatic potential values are anistropically distributed around S atom. The electrostatic potential values are more negative in the π-region of the atom (Fig. 7(left)). According to the electrostatics, for more stabilization, more electronegative potential values encounter the least negative one. This rationalizes the observed H···S–C angle (average = 81°) in the hydrogen bonding interactions. The idea of the anisotropy of electrostatic potential values was observed around carbon attached halogen atoms and utilized to rationalize

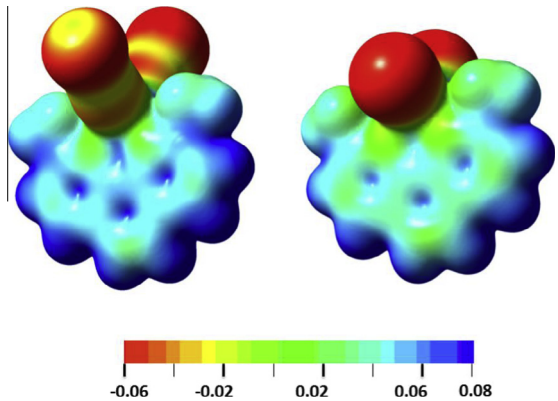

Fig. 7. Calculated electrostatic potential **2** (left) and **1** (right). Energy and charge are expressed in atomic units. The electron density contour iso-value is set to 0.005.

halogen bonding interactions and halogen–halogen contacts [34,35].

UV–visible spectral data

The electronic absorption spectra of the [CoX_2(dmphen)](1–2) complexes are measured at room temperature in acetone (Fig. 8). The solutions of the complexes exhibit multiple absorptions in the UV–visible regions. The ligand displayed typical ligand-centered $\pi \rightarrow \pi^*$ transitions at 240, 280 and 304 nm. Upon coordination with cobalt ions, there are minor changes of these bands but three new bands in the region (555–666 nm) appeared in the visible region for both complexes. For example, complex 1 has two weak transitions at 350, 558 and a strong transition at 642 nm.

The experimental absorption bands for a representative complex (**1**) are assigned using the time-dependent DFT method. Energy level correlations along with the relative percentages of atomic contributions to the lowest unoccupied and highest occupied molecular orbitals of the Co, dmphen and Br ligands have been placed in Table 5. Moreover, the isodensity plots for the HOMOs and LUMOs orbitals are shown in Fig. 9. For complex **1**, the β-spin occupied orbitals mainly take part in electronic transitions. The β-spin and α-spin from HOMO to HOMO−4 have more than 50% Br, while LUMO/+/+4 have more than 50% of Co metal (Table 5). The α-spin LUMO to LUMO+4 have mainly dmphen in character.

Computation of 20 excited states of complex **1** allowed the interpretation of the experimental spectrum in the 200–1000 nm

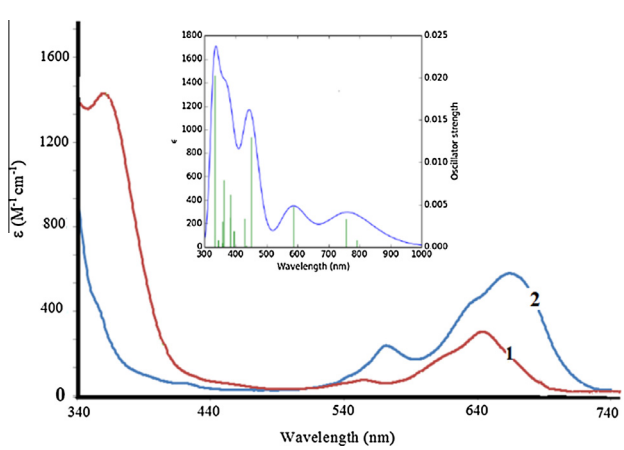

Fig. 8. UV–vis spectrum of the desired complexes **'1** and **2'** in acetone at RT. Inset shows simulated absorption spectrum of complex **1** (green line) based on TD-DFT calculations. (For interpretation of the references to color in this figure legend, the reader is referred to the web version of this article.)

Table 5
DFT energies and composition of selected highest occupied and lowest unoccupied β-spin molecular orbitals of complex **'1** and **2'** expressed in terms of composing fragments.

Complex	Molecular orbital	eV	Co	X	dmphen
1	LUMO+4	−2.01	89	3	9
	LUMO+3	−2.2	27	4	68
	LUMO+2	−2.22	0	0	100
	LUMO+1	−2.59	90	7	3
	LUMO	−3.2	57	7	37
	HOMO	−6.8	10	88	1
	HOMO−1	−6.9	1	55	44
	HOMO−2	−7.05	14	66	20
	HOMO−3	−7.06	9	54	37
	HOMO−4	−7.22	7	92	1
	Millikan charge		0.368	−0.463	−0.428
2	LUMO+4	−1.7	83	11	6
	LUMO+3	−2.09	81	15	5
	LUMO+2	−2.25	45	9	47
	LUMO+1	−2.79	0	0	100
	LUMO	−3.3	21	6	72
	HOMO	−5.4	7	93	0
	HOMO−1	5.63	10	90	0
	HOMO−2	5.66	7	92	1
	HOMO−3	−5.76	5	95	0
	HOMO−4	−7.54	1	0	99
	Millikan charge		0.687	−0.598	−0.402

(Fig. 9). The calculated energy of excitation states and transition oscillator strength (*f*) are shown in Table 6. The absorption spectrum of **1** was simulated using Gauss Sum software [30] based on the obtained TD-DFT results. Both the experimental UV–Visible and its simulated absorption spectra in acetone shown in Fig. 4 are in acceptable agreement.

On the basis of its intensity and position, the high intensity and energy band at 240 nm (332 nm, calculated) is result from H-5(α) and H-5(β) to L(α) and L(β) which are mainly dmphen in character, thus this band is assigned as to dmphen(π) → dmphen(π∗) transition. 357 the band centered at 357 nm (499 nm, calculated) is resulted from H-1(β) which is mainly bromide in character, thus this band is assigned as bromide (Pπ) → dmphen(π∗) transition (89%). The weak transition at 558 nm (586 nm, calculated) is resulted from H-8(β) and H(β) to L+4(β) which are mainly Co in character thus this band is assigned to d–d transition. The lowest energy band at 642 nm (756 nm, calculated) is resulted from H-9(β) which is mainly Co in character to L+1(β) which is mainly dmphen in character, thus this band is assigned to MLCT transition.

For complex **2**, all bands in the visible region are shifted to a lower energy relative to complex **1**. The shift can be explained in terms of the formal charge on the central metal and the type of the ligand for both complexes. The high value of effective nuclear charge of cobalt ion in **2** (Table 5) can be explained on the basis of electronic effects and charge distribution in both complexes. It is known that Co(II) ion has an almost filled non-bonding t2g orbital capable to overlap with the antibonding π^*-orbital of 1,l0 phenanthroline [36]. The extent of $d\pi$–$p\pi^*$ overlapping is strongly influenced by the nature of ligands attached to it. In complex **2**, cobalt ion is bonded with thiocyanate through nitrogen (not through sulfur). The strong dative π-bonding (dπ–pπ) in Co–NCS bond renders the nonbonding t2g metal orbitals less available for the overlap with 1,l0 phenanthroline π levels [37]. So there will be a large polarization of the charge of cobalt ion towards thiocyanate ligand with the resultant more effective nuclear charge on cobalt ion (Table 5). The theoretical predictions of molecular orbital theory will be applied to explain the spectral features. Now we will deal with the positions of principal absorption maxima. The shift of principal absorption maxima depends on the type of the overlap between metal atom and the ligand orbitals. The greater

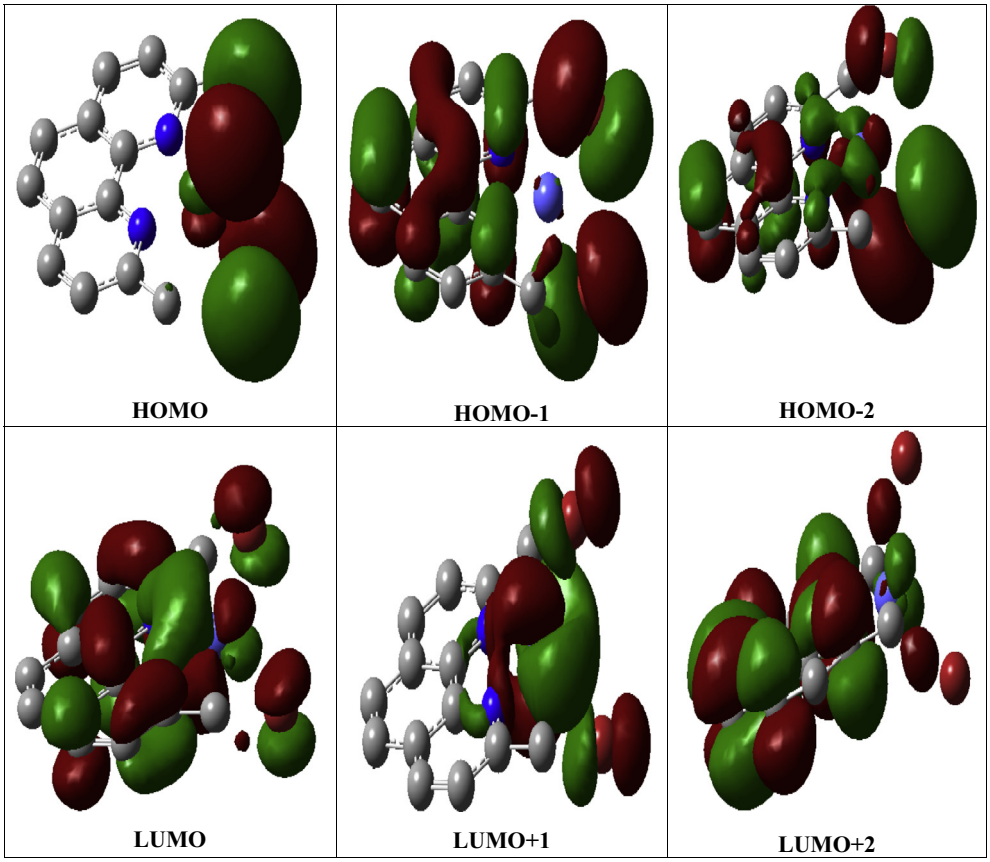

Fig. 9. Isodensity plots of some selected MOs (β-spin) of complex **1**.

Table 6
Computed excitation energies (nm), electronic transition configurations and oscillator strengths (*f*) for complexes **'1** and **2'**.

	nm	Osc, str.	Major contribs
1	756	0.0033	H-9(β) → L+1(β) (53%), H-3(β) → L+1(β) (13%), H-2(β) → L+1(β) (24%)
	586	0.0048	H-11(β) → L+4(β) (17%), H-8(β) → L+4(β) (35%), H(β) → L+4(β) (31%)
	499	0.013	H-1(β) → L(β) (89%)
	429	0.0034	H-3(β) → L(β) (49%), H-2(β) → L(β) (30%)
	395	0.0019	H-9(β) → L(β) (23%), H-3(β) → L(β) (26%), H-2(β) → L(β) (42%)
	383	0.0062	H-3(β) → L+1(β) (19%), H-2(β) → L+1(β) (12%), H-1(β) → L+1(β) (62%)
	382	0.0035	H-5(α) → L (α) (13%), H-1(α) → L+1(α) (10%), H-5(β) → L(β) (50%)
	361	0.0079	H-1(α) → L(α) (48%)
	332	0.0203	H-5(α) → L(α) (33%), H-2(α) → L(α) (16%), H-5(β) → (β) (25%)
2	658	0.0062	H-7(β) → L+1(β) (63%), H-1(B) → L+1(B) (29%)
	616	0.021	H-6(β) → L+4(B) (35%), H(β) → L+4(β) (34%)
	468	0.037	H-2(β) → L(β) (94%)
	444	0.0464	H-7(β) → L(β) (13%), H-1(β) → L(β) (78%)
	391	0.0719	H-2(β) → L+1(β) (96%)
	379		H-5(α) → L(α) (16%), H-4(α) → L+1(α) (11%), H-5(β) → L(β) (54%)
	368	0.0037	H-2(α) → L(α) (98%)

the overlap of the metal and the ligand orbital, the more stable are bonding molecular orbitals and hence the more unstable the antibonding orbitals [38]. In both complexes, the β-spin occupied orbitals mainly take part for the electronic transitions in the visible region while a mixture of α and β-spin are responsible for the electronic transition in the Uv-region (Table 6). The red shift for the visible absorption maxima and the high Co-(dmphen) covalent bond character for $CoBr_2$(dmphen) is in agreement by the large difference in the energy between bonding and antibonding β molecular orbitals (Table 5) for complex **1**. For complex **2**, The strong π-bonding (dπ–pπ) interaction for Co–NCS bond makes the t2g metal orbitals less available for the overlap with 1,l0 phenanthroline π levels as in the case of complex **1** [37].

*Antibacterial activity of complexes **1–2***

Qualitative antibacterial screening of the complexes produced in this study showed high antibacterial activity of the two tested compounds against both gram positive (*S. aureus* and *Bacillus subtilis*) and gram negative (*E. coli* and *P. aeruginosa*) bacterial strains as indicated by the presence of large inhibition zones (Table 7). The inhibition zones for the two complexes were higher than the zones produced by the negative control or the ligand. This indicates that the obtained antimicrobial effects are mainly due to the complexes under investigation. The highest antimicrobial effect for all complexes was observed against *Bacillus subtilis* with inhibition zones around 23 mm which is slightly higher than the

Table 7
Antimicrobial activity of the complexes (1 mg/ml) against various microbial strains (inhibition zones in mm).

Compound	Microbial strains			
	Escherichia coli	*Staphylococcus aureus*	*Pseudomonas aeruginosa*	*Bacillus subtilis*
Complex **1**	17	18	15	23
Complex **2**	18	18	22	22
Ligand	0	2	2	3
Tetracycline	20	24	22	19
1% DMSO	0	0	0	0

zone obtained by the positive control (tetracycline) which showed an inhibition zone of 21 mm against the same bacterial strain. Different complexes exhibited different antibacterial activity against *E. coli*. The highest activity was for complex **3** then complex **1** with inhibition zones of 18, and 16 mm, respectively. The two complexes were active against *S. aureus* with inhibition zones around 18 mm. On the other hand, different activities were observed against *P. aeruginosa* with inhibition zones of 22 and 15 mm for complex 3 and 1, respectively. Our results are consistent with the previous findings activity for cobalt complexes against an array of bacteria including *Bacillius subtilis*, *S. aureus*, *E. coli*, and *Enterobacter fecalis* [39,40]. The broad antibacterial spectrum of our complexes can be explained by the ability of these complexes to bind bacterial DNA causing DNA fragmentation. This mode of action was also observed with other cobalt complexes [41]. However, further testing is needed to clearly understand the mechanism of the action of these complexes and the range of microbes that can be inhibited using them.

Conclusions

Two new tetrahedral neutral Co(II) complexes of general formula [CoX_2(dmphen)] were prepared. These complexes were characterized by EA, UV–vis, FT-IR, TG/DTA, CV and X-ray single crystal. Both complexes exhibited significant antibacterial activity against different gram negative and positive human pathogens. The calculated electrostatic potentials were found effective to rationalize the self-assembly of the two complexes. In **2**, the electrostatic potential values are anistropically distributed around sulfur atom, the electrostatic potential is less negative a long C–S bond than the π-region of the S atom.

Supplementary material

Crystallographic data for complexes **'1** and **2'** have been deposited with the Cambridge Crystallographic Data Centre as supplementary publication number CCDC 0001000198333 and 1014369 respectively. Copies of this information may be obtained free of charge via www.ccdc.cam.ac.uk/conts/retrieving.html (or from the CCDC, 12 Union Road, Cambridge CB2 1EZ, UK; fax: +44 1223 336033; e-mail: deposit@ccdc.cam.ac.uk).

Acknowledgements

M. Al-Noaimi and I. Warad would like to thank The Hashemite University, Jordan and AN-Najah National University for their research support. The authors are thankful to the IOE, Vijnana Bhavana, University of Mysore, Mysore, for providing the single-crystal X-ray diffractometer facility.

References

[1] M. Al-Noaimi, M. AlDamen, Inorg. Chim. Acta 387 (2012) 45.
[2] M. Al-Noaimi, M. El-khateeb, S. Haddad, M. Sunjuk, R.J. Crutchley, Polyhedron 27 (2008) 3239.
[3] J.D. Lee, Concise Inorganic Chemistry, forth ed., Chapman and Hall, London, 1991, p. 607.
[4] M.S. Bapna, S. Mukherjee, R.J. Murphy, Oral Rehabit. 19 (2007) 111.
[5] K.E. Erkkila, D.T. Odom, J.K. Barton, Chem. Rev. 99 (1999) 2777.
[6] (a) M. Grätzel, Inorg. Chem. 44 (2005) 6841;
(b) K.K. Bania, R.C. Deka, J. Phys. Chem. C 116 (2012) 14295.
[7] D.S. Sigman, A. Mazumder, D.M. Perrin, Chem. Rev. 93 (1993) 2295.
[8] N.J. Turro, J.K. Barton, D.A. Tamalia, Acc. Chem. Res. 24 (1991) 332.
[9] A.M. Pyle, J.K. Barton, Prog. Inorg. Chem. 38 (1990) 413.
[10] (a) M. Murrie, Chem. Soc. Rev. 39 (2010) 1986;
(b) S. Hayami, Y. Komatsu, T. Shimize, H. Kamihata, Y.H. Lee, Coord. Chem. Rev. 255 (2011) 1981.
[11] D.-F. Weng, Z.-M. Wang, S. Gao, Chem. Soc. Rev. 40 (2011) 3157.
[12] G.E. Kostakisa, S.P. Perlepesb, V.A. Blatovc, D.M. Proserpiod, A.K. Powella, Coord. Chem. Rev. 256 (2012) 1246.
[13] S. Utsuno, Y. Yosbikawa, A. Tatehate, H. Yamatera, Chem. Sot. Jpn. 54 (1981) 1814.
[14] E.C. Niederhaffer, A.E. Martell, P. Rudolf, A. Clearfield, Inorg. Chem. 21 (1982) 3734.
[15] (a) I. Warad, A. Boshaala, S.I. Al-Resayes, S.S. Al-Deyab, M. Rzaigui, Acta Cryst. Acta Cryst. E67 (2011) m1650;
(b) I. Warad, A. Boshaala, S.I. Al-Resayes, S.S. Al-Deyab, M. Rzaigui, Acta Cryst. E67 (2011) m1846;
(c) I. Warad, M. Al-Noaimi, S.F. Haddad, R. Othman, Acta Cryst. E69 (2013) m109.
[16] (a) I. Warad, B. Hammouti, T. Ben Hadda, A. Boshaala, S.F. Haddad, Res. Chem. Intermed. 39 (2013) 4011;
(b) I. Warad, M. Al-Ali, B. Hammouti, T. Ben Hadda, R. Shareiah, M. Rzaigui, Res. Chem. Intermed. 39 (2013) 2451.
[17] (a) A.S. Aldwayyan, F.M. Al-Jekhedab, M. Al-Noaimi, B. Hammouti, T.B. Hadda, I. Warad, M. Suleiman, Int. J. Electrochem. Sci. 8 (2013) 10506.
[18] X1-Bruker APEX2, SADABS, SAINT-Plus and XPREP. Bruker AXS Inc., Madison, Wisconsin, USA, 2009.
[19] CrysAlisPro, Agilent Technologies, Version 1.171.35.11 (Release 16–05–2011CrysAlis171.NET) (Compiled 16.05.11, 17:55:39).
[20] SHELXTL (XPREP, XL, XP, XCIF), version, Bruker AXS Inc., Madison, WI, 2002.
[21] J.K. Hurst, Coord. Chem. Rev. 249 (2005) 313.
[22] D. Chatterjee, A. Mitra, R.E. Shepherd, Inorg. Chim. Acta 357 (2004) 980.
[23] C. Lee, W. Yang, R.G. Parr, Phys. Rev. B 37 (1988) 785.
[24] M.J. Frisch, G.W. Trucks, H.B. Schlegel, G.E. Scuseria, M.A. Robb, J.R. Cheeseman, G. Scalmani, V. Barone, B. Mennucci, G.A. Petersson, H. Nakatsuji, M. Caricato, X. Li, H.P. Hratchian, A.F. Izmaylov, J. Bloino, G. Zheng, J.L. Sonnenberg, M. Hada, M. Ehara, K. Toyota, R. Fukuda, J. Hasegawa, M. Ishida, T. Nakajima, Y. Honda, O. Kitao, H. Nakai, T. Vreven, J.A. Montgomery, Jr., J.E. Peralta, F. Ogliaro, M. Bearpark, J.J. Heyd, E. Brothers, K.N. Kudin, V.N. Staroverov, R. Kobayashi, J. Normand, K. Raghavachari, A. Rendell, J.C. Burant, S.S. Iyengar, J. Tomasi, M. Cossi, N. Rega, J.M. Millam, M. Klene, J.E. Knox, J.B. Cross, V. Bakken, C. Adamo, J. Jaramillo, R. Gomperts, R.E. Stratmann, O. Yazyev, A.J. Austin, R. Cammi, C. Pomelli, J.W. Ochterski, R.L. Martin, K. Morokuma, V.G. Zakrzewski, G.A. Voth, P. Salvador, J.J. Dannenberg, S. Dapprich, A.D. Daniels, O. Farkas, J.B. Foresman, J.V. Ortiz, J. Cioslowski, D.J. Fox, Gaussian 09, Revision A.1, Gaussian Inc, Wallingford CT, GaussView5.0.9, Gaussian: Pittsburgh, PA, 2009.
[25] P.J. Hay, W.R. Wadt, J. Chem. Phys. 82 (1985) 270.
[26] R. Bauernschmitt, R. Ahlrichs, Chem. Phys. Lett. 256 (1996) 454.
[27] M.K. Casida, C. Jamorski, K.C. Casida, D.R. Salahub, J. Chem. Phys. 108 (1998) 4439.
[28] R.E. Stratmann, G.E. Scuseria, M.J. Frisch, J. Chem. Phys. 109 (1998) 8218.
[29] M. Cossi, N. Rega, G. Scalmani, V. Barone, Comput. Chem. 24 (2003) 669.
[30] N.M. O'Boyle, A.L. Tenderholt, K.M. Langner, J. Comput. Chem. 29 (2008) 839.
[31] M. Lalia-Kantouri, C.D. Papadopoulos, A.G. Hatzidimitriou, M.P. Sigalas, M. Quirós, S. Skoulika, Polyhedron 52 (2013) 1306.
[32] F.F. Awwadi, S.F. Haddad, B. Twamley, R.D. Willett, CrystEngComm 14 (2012) 6761.
[33] O.V. Dolomanov, L.J. Bourhis, R.J. Gildea, J.A.K. Howard, H. Puschmann, J. Appl. Cryst. 42 (2009) 339.
[34] E. Bosch, C.L. Barnes, Cryst. Growth Des. 2 (2002) 299.
[35] F.F. Awwadi, R.D. Willett, K.A. Peterson, B. Twamley, Chem. Eur. J. 12 (2006) 8952.
[36] B.R. James, R.J.P. Williams, J. Chem. Soc. (1961) 2007
[37] H.C.A. King, E. Körös, S.M. Nelson, J. Chem. Soc. (1963) 5449
[38] G.L. Glen, C.G. Dodd, J. Appl. Phys. 39 (1968) 5372.
[39] E.L. Chang, C. Simmers, D.A. Knight, Pharmaceuticals 3 (2010) 1711.
[40] M. Kaya, C. Yenikaya, A.T. Colak, F. Colak, Russ. J. Gen. Chem. 78 (2008) 1808.
[41] R.S. Kumar, S. Arunachalam, Biophys. Chem. 136 (2008) 136.